ADVANCED OPTICAL MATERIALS
www.advopticalmat.de

High-Performance Transmission Structural Colors Generated by Hybrid Metal-Dielectric Metasurfaces

Bo Yang, Wenwei Liu, Duk-Yong Choi, Zhancheng Li, Hua Cheng, Jianguo Tian,* and Shuqi Chen**

Despite structural colors based on metasurfaces drawing enormous attentions due to the high resolutions and superior durability, few researches focus on transmission colors in RGB model with high saturation because high-monochromaticity transmission peak is hard to be realized. Herein, a strategy of high-performance transmission structural colors in RGB model with high saturation, full hue, high efficiency, easy manufacturability, and polarization independence by means of Al-Si_3N_4 nanoblocks deposited on glass substrate is proposed. The coupling between Wood's anomaly and Mie lattice resonance is capable of introducing magnetic-dipole and electric-quadrupole resonances, creating enhanced resonant peak with full width of half maximum (FWHM) of 50 nm and efficiency of over 70% in transmission mode. High-saturation transmission colors occupying 150% standard RGB (sRGB) space can be obtained for the first time by tailoring the geometric parameters. Besides, it is also demonstrated that the hybrid nanostructures can realize full-hue colors with constant resolutions, which is significant for imaging applications. The designed method has potential for further extending the applications of transmission colors.

1. Introduction

Structural colors, deriving from the interference between light and structures, have been a scientific hotspot for advanced displays, high-end images, anti-counterfeiting technology, and data storage for several years.[1–6] With the development of nanofabrication technology, structural colors generated by plasmonic[1–3,7–13] or dielectric[14–21] metasurfaces exhibiting superior resolutions and high durability have been drawing tremendous interest in the visible spectra. Up to now, there have been wealthy studies on structural colors consisting of static colors[14–21] and tunable colors[22–24] in reflection mode with modulation of saturation, hue, and brightness. For example, in our previous work, the wide static colors exceeding 170% sRGB (standard RGB) space can be obtained by utilizing index matching among trilaminar dielectric nanoblocks to deeply modulate multipolar modes of reflection resonance.[19] Carrillo et al. proposed switchable phase-change metasurface resonant absorber to selectively absorb colors in the crystalline phase, providing potential development in front-end color displays, and color electronic signage.[23]

For the structural colors in transmission mode, the majority of previous studies mainly focused CMYK color model since all-dielectric nanostructures can readily generate high-monochromaticity transmission valley.[10,17–19,25–29] Realizing of high-performance transmission colors in RGB color model remains a challenge. **Table 1** presents several representative designs to realize transmission colors in RGB model.[30–38] In the infancy, the strategy of arrayed nanoholes or nanoslits in optically-thick metallic films was extensively used to provide surface-plasmon enhanced transmission.[20–32] But only broad spectra with low efficiency and monochromaticity can be obtained because metallic materials hold high ohmic loss. In order to improve the quality of transmission spectra, the designs of metal-dielectric hybrid nanostructures were applied to realize structural colors with higher saturation.[33–38] For instance, Yun et al. proposed a bi-layer hybrid metasurface consisting of Al nanogratings and asymmetrical amorphous Si nanorods.[35] Although the cavity effects between bi-matasurfaces can lead to unprecedented high-saturation colors taking up 90% sRGB space in the simulation, the low efficiency of about 16% and complicated

B. Yang, W. Liu, Z. Li, H. Cheng, J. Tian, S. Chen
The Key Laboratory of Weak Light Nonlinear Photonics
Ministry of Education
School of Physics and TEDA Institute of Applied Physics
Renewable Energy Conversion and Storage Center
Nankai University
Tianjin 300071, China
E-mail: hcheng@nankai.edu.cn; jjtian@nankai.edu.cn; schen@nankai.edu.cn

The ORCID identification number(s) for the author(s) of this article can be found under https://doi.org/10.1002/adom.202100895.

DOI: 10.1002/adom.202100895

D.-Y. Choi
Laser Physics Centre, Research School of Physics and Engineering
Australian National University
Canberra, Australian Capital Territory 2601, Australia

S. Chen
The Collaborative Innovation Center of Extreme Optics
Shanxi University
Taiyuan, Shanxi 030006, China

S. Chen
The Collaborative Innovation Center of Light Manipulations and Applications
Shandong Normal University
Jinan 250358, China

Table 1. Representative works on transmission colors in RGB color model.

	Representative works	FWHM	Saturation[/sRGB]	Efficiency
Nanoholes	Ref. [30]	≈140 nm	—	≈40%
Nanocavities	Ref. [33]	≈100 nm	—	≈60%
Bi-layer structures	Ref. [35]	≈60 nm	~ 90%	≈16%
Nanogratings	Ref. [36]	≈70 nm	~ 80%	≈70%
Meta-dielectric structures	This work	≈50 nm	~ 150%	≈70%

fabrication process seriously hinder practical applications. Lee et al. remarkably demonstrated hybrid TiO_2-Ag core-shell nanogratings with high efficiency of about 70% as transmissive type pixels can generate ultrahigh resolutions exceeding 100 000 dots-per-inch and wide color gamut occupying about 80% sRGB space, resulting from reduced scattering at Mie resonances of electric dipolar.[36] However, the transmissive color pixels only operated at the fixed polarization state on account of high polarization sensibility of nanogratings. Hence, it is inevitable and imperative to develop a designed strategy of symmetrical nanostructures with high efficiency and simple fabrication process to realize high-saturation and full-hue transmission colors in RGB model, which is crucial for practical applications, such as displays, images, color printing, data storage, and so on.

Here, we proposed the high-performance transmission structural colors with high saturation, full hue, high efficiency, easy manufacturability, and polarization independence by hybrid metal-dielectric metasurfaces composing of symmetrical Al-Si_3N_4 nanoblocks on glass substrate. The coupling between Wood's anomaly of Al nanoblocks and Mie lattice resonance of Si_3N_4 nanoblocks can introduce magnetic-dipole and electric-quadrupole resonances, leading to superior transmission peak with high efficiency of over 70% and high monochromaticity with full width of half maximum (FWHM) of 50 nm (Table 1). We theoretically and experimentally demonstrated full-hue and high-saturation transmission colors in RGB model taking up wide gamut of about 150% sRGB space (the widest color space against precedent as far as we know) in simulation via tuning period from 250 to 390 nm. More interesting, full-hue colors including blue, green, and red with constant resolutions are significantly realized by utilizing the hybrid metal-dielectric nanostructures when the period is fixed at 380 nm, implying the nanostructures have promising potentials for imaging and displaying applications.

2. Results and Discussion

2.1. The Mechanism of Hybrid Metasurfaces

Figure 1 presents the schematic diagram of the proposed hybrid metal-dielectric metasurface, in which Si_3N_4 and Al nanoblocks successively deposited on glass substrate. When white light source incidents on the side of glass substrate, iridescent colors can be observed from the side of nanoblocks with varying geometric parameters. The height of Al and Si_3N_4 layers are defined as $H_1 = 60$ nm and $H_2 = 150$ nm, respectively. The gap

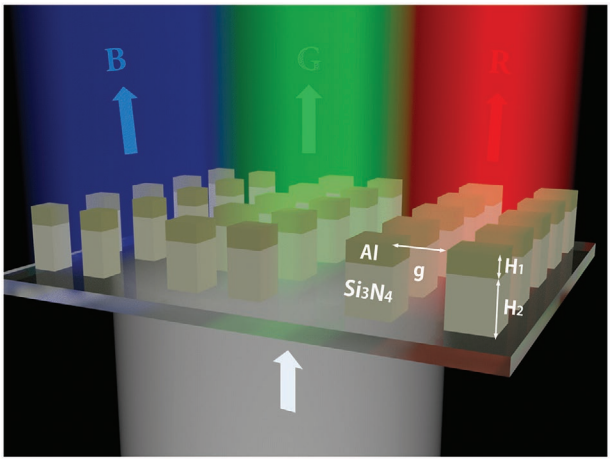

Figure 1. Schematic of hybrid metal-dielectric mateasurfaces. 60 nm thick Al and 150 nm thick Si_3N_4 successively stack on glass substrate. The white light incident on the glass substrate and structural colors emerge from the side of nanoblocks.

size (g) is expressed as the difference value between the period (P) of the unit cell and the width (W) of the nanoblock, namely, $g = P - W$. Al as an abundant natural material is a good candidate in our design since the interband transition lies outside the visible and near-UV spectral bands, enabling strong plasmon resonances.[7] Besides, Al materials has uniform reflectivity and is compatibility with complementary metal oxide semiconductor (CMOS) process.[25] As the oxide film formed on the surface of Al materials can prevent further oxidation of Al, the effects of oxidation of Al in the ambient on long-term stability of colors can be negligible.

To investigate the physical mechanisms of transmission resonant peak, we respectively analyzed the optical characteristics of the mono-layer Al nanostructures, mono-layer Si_3N_4 nanostructures and the hybrid Al-Si_3N_4 nanostructures in **Figure 2**. Figure 2a gives the simulated transmission spectra of the mono-layer Al nanostructures with optical thickness of 60 nm and gap size of 80 nm for different periods. Taking the period of 330 nm as an example, the highly suppressed transmission can be selectively realized at wavelength of 520 nm (blue dot) resulting from surface plasmon resonances (SPRs).[25] At the shorter wavelength of 495 nm, a narrow and sudden transmission peak (grey dot) is excited on account of Wood's anomaly for Al-glass interface and air-Al interface, which occurs around Rayleigh wavelengths when the diffraction order is tangent to the plane of grating according to the equation:[39–41]

$$\lambda_{WA} = \frac{P}{\sqrt{i^2 + j^2}} \sqrt{\varepsilon_d} \tag{1}$$

where i and j are integers representing diffraction orders, and ε_d is the permittivity of dielectric materials. When the periods are fixed at 270, 330, and 380 nm, the calculated response wavelengths of Wood's anomaly with the diffraction order (1,0) are 405, 495, and 570 nm, which are exactly in accordance with simulated results. The asymmetric Fano profiles of the transmission spectra result from a superimposition of resonant and nonresonant contributions to the zero diffraction order.[39]

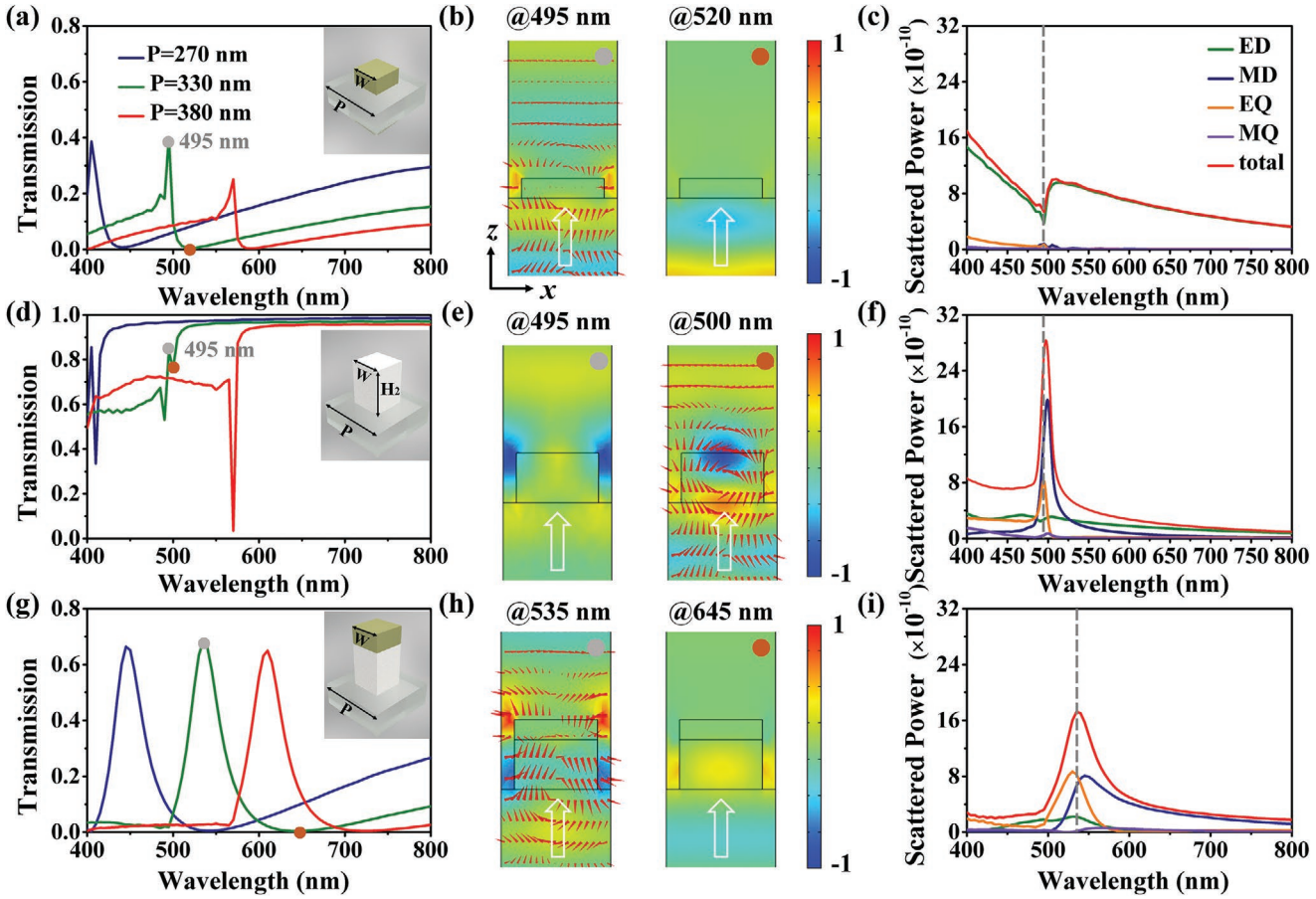

Figure 2. Physical mechanisms of hybrid Al-Si_3N_4 metasurfaces. a,d,g) Simulated transmission spectra for a) mono-Al, d) mono-Si_3N_4, and g) Al-Si_3N_4 nonoblocks when period is fixed at 270 nm (blue curve), 330 nm (green curve), and 380 nm (red curve), respectively. Insets show the illustration of unit cells. b,e,h) The distribution of electric field E_x for b) mono-Al, e) mono-Si_3N_4, and h) Al-Si_3N_4 nonoblocks. The grey and orange dots represents distinct response wavelengths in (a), (d), and (g). c,f,i) Multipolar decomposition of scattering cross section in terms of ED, MD, EQ, and MQ for c) mono-Al, f) mono-Si_3N_4, and i) Al-Si_3N_4 nonoblocks for fixed period of 330 nm. The dashed lines locate at the resonant wavelengths of transmission spectra.

According to the general multipole scattering theory,[42] we decomposed the scattering cross section into electric dipole (ED), magnetic dipole (MD), electric quadrupole (EQ), and magnetic quadrupole (MQ). In the case of harmonic excitation exp ($i\omega t$), the total scattering cross-section can be expressed as:

$$I = \frac{2\omega^4}{2c^3}|\mathbf{P}|^2 + \frac{2\omega^4}{2c^3}|\mathbf{M}|^2 + \frac{\omega^6}{5c^5}\sum|Q_{\alpha\beta}|^2 + \frac{\omega^6}{40c^5}\sum|M_{\alpha\beta}|^2 \quad (2)$$

where $c$is the speed of light in the vacuum. **P**, **M**, $Q_{\alpha}\beta$ and $M_{\alpha}\beta$ represent ED, MD, EQ and MQ moments, respectively. As shown in Figure 2c, ED plays a leading role for plasmon resonances within mono-layer Al nanostructures. Since electric-dipolar resonances hold non-directionality of scattering, namely, the radiation of electric field is strong in both the substrate (reflection) and the air (transmission). The transmission efficiency is <0.4 within mono-layer Al nanostructures.[43] To further enhance transmission efficiency and suppress reflection efficiency, it is essential to break the symmetric scattering by introduce anti-symmetric terms, which corresponds to an effective magnetic resonances or higher order resonances.[43,44] Thus, we added a layer of Si_3N_4 nanoblocks with 150 nm height underneath Al nanoblocks to form the hybrid Al-Si_3N_4 nanostructures. On account of relatively moderate refractive index of Si_3N_4 material ($n_{Si_3N_4} \approx 2.0$), the electric-field profile would spread into nanogaps and substrate, signifying strong coupling between the resonators and the substrate, as the distribution of electric field shown in Figure 2e. For periodic arrays Si_3N_4 nanoblocks, the electromagnetic coupling between nonoblocks and substrate can support strong magnetic dipole lattice resonance in the vicinity of Rayleigh wavelengths (Figure 2f).[23] The coupling between Wood's anomaly of Al layer and magnetic dipole lattice resonance of Si_3N_4 layer is able to excite strong magnetic-dipolar and electric-quadrupole resonances (Figure 2i).[40] As the transmission spectra shown in Figure 2g, the magnetic-dipolar, electric-quadrupole, and slight electric-dipolar resonances can break the symmetric scattering, resulting in high-monochromaticity spectra with enhanced transmission efficiency. In a word, the higher-efficiency and higher-monochromaticity spectra in transmission mode can be obtained by using the hybrid Al-Si_3N_4 nanostructures. By virtue of changing the periods and widths, the resonant peak with about 70% efficiency and around 50 nm FWHM can be flexibly tuned over the visible spectra. That means the proposed design

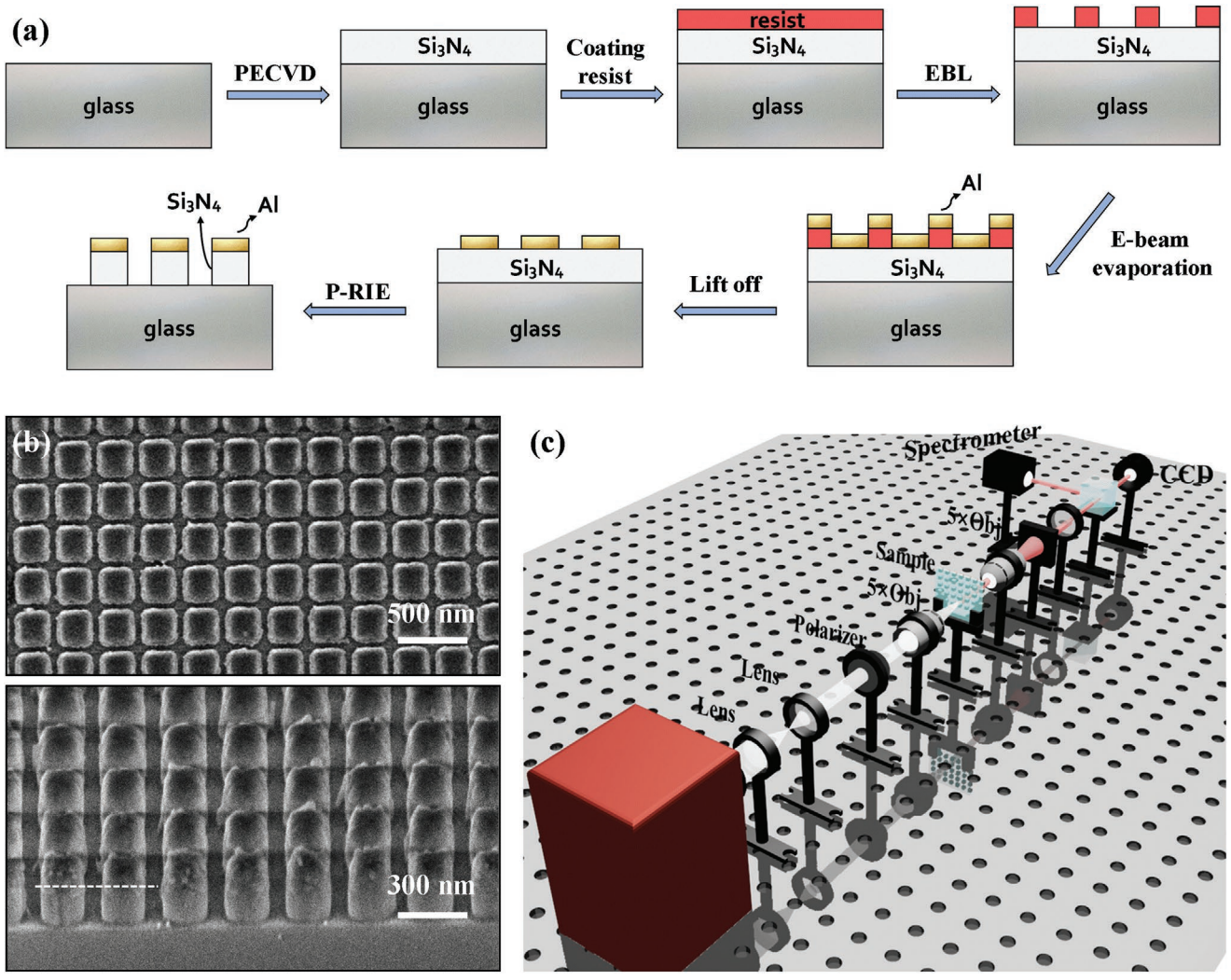

Figure 3. a) Fabrication process of metal-dielectric metasurfaces. The proposed nanoblocks array is fabricated by EBL and plasma etching. b) The top-view and side-view SEM images of the Al-Si_3N_4 metasurface, respectively. c) The schematic of home-built setup to measure transmission spectra and capture color patterns. The apertures of objective are 0.13.

of hybrid Al-Si_3N_4 nanostructures is capable of generating high-efficiency structural colors with high saturation and full hue in transmission mode.

2.2. Experimental Results

In order to verify our designs, we fabricated the hybrid Al-Si_3N_4 samples by electron beam lithography (EBL) and plasma etching. As the flow chart of the fabrication process shown in **Figure 3**a, 150 nm-thick layer of Si_3N_4 was deposited on glass substrate in a plasma-enhanced chemical vapor deposition system (PECVD) from Plasmalab 100 (Oxford). A square array was printed by EBL (Raith150) after a positive electron-beam resist (ZEP520A from Zeon Chemicals) was coated on the layer. During the process of EBL, a thin layer of e-spacer consisting of spin-coatable water-based liquid (300Z from Showa Denko) was used to prevent charging. 70 nm thick Al as etch mask was deposited by e-beam evaporation (Temescal BJD-2000), accompanied by a lift-off process in which the sample was soaked in a resist remover (ZDMAC from ZEON Co.). Using CHF_3 gas, the nanoblocks were etched in inductively coupled plasma-reactive ion etching (P-RIE) (Plasmalab System 100, Oxford). Due to high etch selectivity of Al to Si_3N_4 in the plasma (estimated around 30), there remains about 60 nm-thick Al on Si_3N_4 nanoblocks.The SEM images in Figure 3b present the details of fabricated sample in top view and side view, respectively. It is clear to see that the isolated nanoblock is consist of Si_3N_4 layer and Al layer in succession. Compared with the fabrication process of all- dielectric nanostructures by EBL, this fabrication method leaved out the last step of removing residual Al mask, leading to a more convenient fabrication process. We utilized the home-built setup in Figure 3c to measure transmission spectra and color patterns. Bromine tungsten (Br-W) lamp as light source can provide high-intensity and stable white light ranging from 400 to 800 nm. The samples were set between two reversed

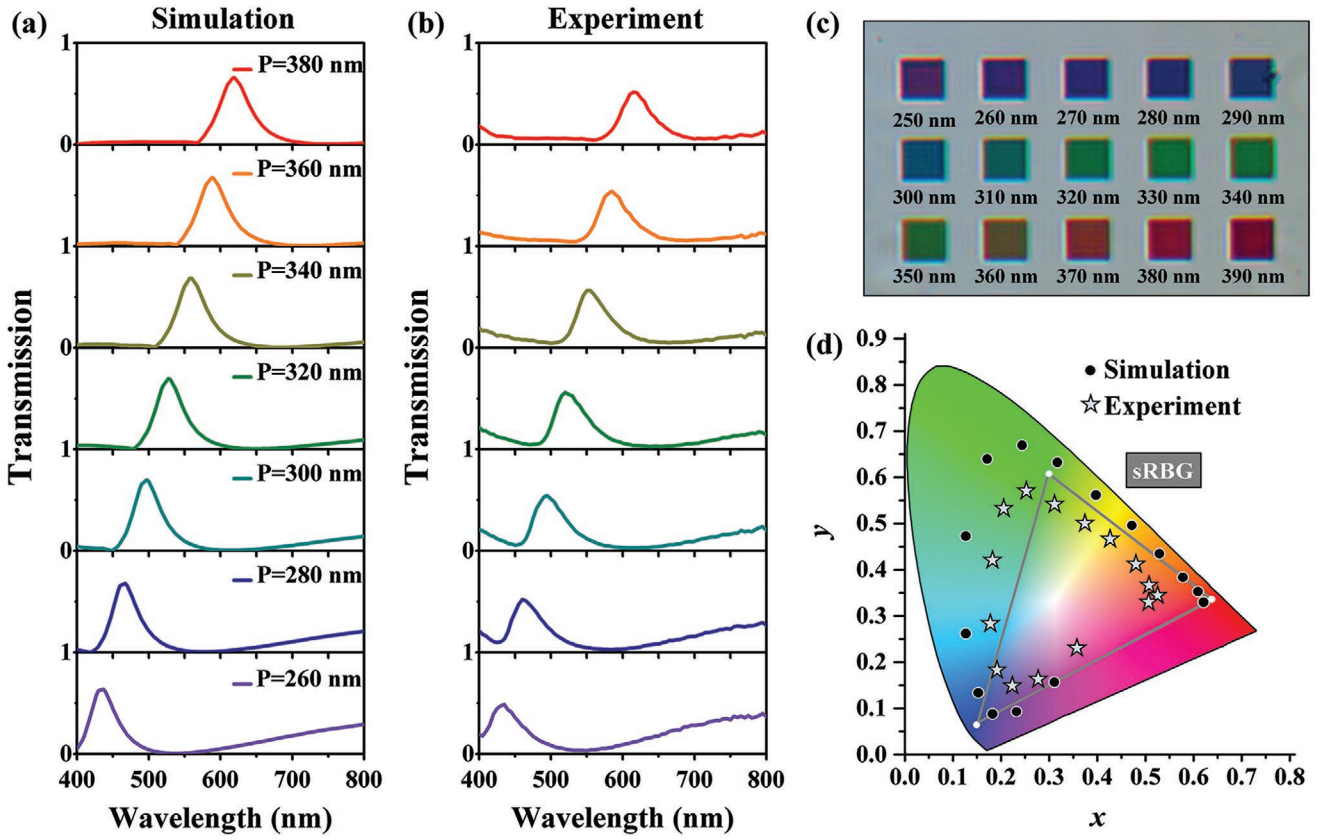

Figure 4. Transmission colors with high saturation and full hue when the gap size is fixed at 80 nm for Al-Si_3N_4 metasurfaces. a) Simulated and b) Measured transmission spectra with increasing period varying from 260 to 380 nm with 20 nm increment. c) Measured color palette in bright field captured by CCD camera. The period changed from 250 to 390 nm with 10 nm increment. d) Corresponding chromaticity values in 1931 CIE diagram for simulated (black dots) and measured (grey stars) spectra, respectively. The triangle represents sRGB color space.

5× objectives (numerical aperture of 0.13) to focus light and magnify images, respectively. Taking advantage of this setup, the transmission spectra and color patterns of 30 μm side-length sample can be readily captured by spectrometer and charge-coupled device (CCD) camera.

Figure 4 shows the measured and simulated transmission spectra of the hybrid Al-Si_3N_4 nanostructures to generate high-performance structural colors. Trading off high saturation of structural colors and accessibility of practical fabrication, we set the gap size as constant of 80 nm when the period changes. Figure 4a exhibits simulated spectra in transmission mode, indicating that the resonant peak with stable efficiency and high monochromaticity can be flexibly tuned from 430 to 620 nm by increasing period from 260 to 380 nm with 20 nm increments. The measured spectra in Figure 4b are in good agreement with the simulated results in terms of resonant wavelength and spectral lineshape, verifying our theoretical predictions. The slight peak appearing at the lower wavelengths is attributed to the imperfect sample fabrication, that is, the top-layer Al nanoblocks hold fillet angle other than right angle on the edge. In the experiment, the resonant peak performs a redshift from 425 to 615 nm with efficiency of over 50% when the periods gradually increase. Wide gamut ranging from purple, blue, green to red is captured by CCD camera in Figure 4c, which are iridescent and vivid. To quantificationally perform the gamut, we calculated the tristimulus values on the International Commission on Illumination (CIE) 1931 chromaticity diagram in Figure 4d, where the black dots and grey stars respectively present the simulated and measured coordinates when the period changes from 250 to 390 nm. The simulated gamut can take up about 150% sRGB color space, implying that the transmission colors own high saturation. Although the measured gamut is smaller than that in simulation due to the fabrication defects containing roughness of surface and deformation of shape, etc., the measured results reasonably agree well with the simulated results. We experimentally proved the high-performance transmission colors within hybrid Al-Si_3N_4 nanostructures.

Realization of full-hue structural colors with constant resolutions is of great significance for displaying applications. We demonstrate that the hybrid Al-Si_3N_4 nanostructures can realize structural colors with full hue when the period is fixed at 380 nm in **Figure 5**. Figure 5a and 5b show the simulated and measured transmission spectra when the gap size decreases from 240 to 80 nm with 20 nm decrement, respectively. There is a wide-range redshift for resonant peak spanning from 460 to 620 nm since the smaller gap size holds the larger effective index. The increasing filling fraction of hybrid nanostructures can lead to the enhanced optical path

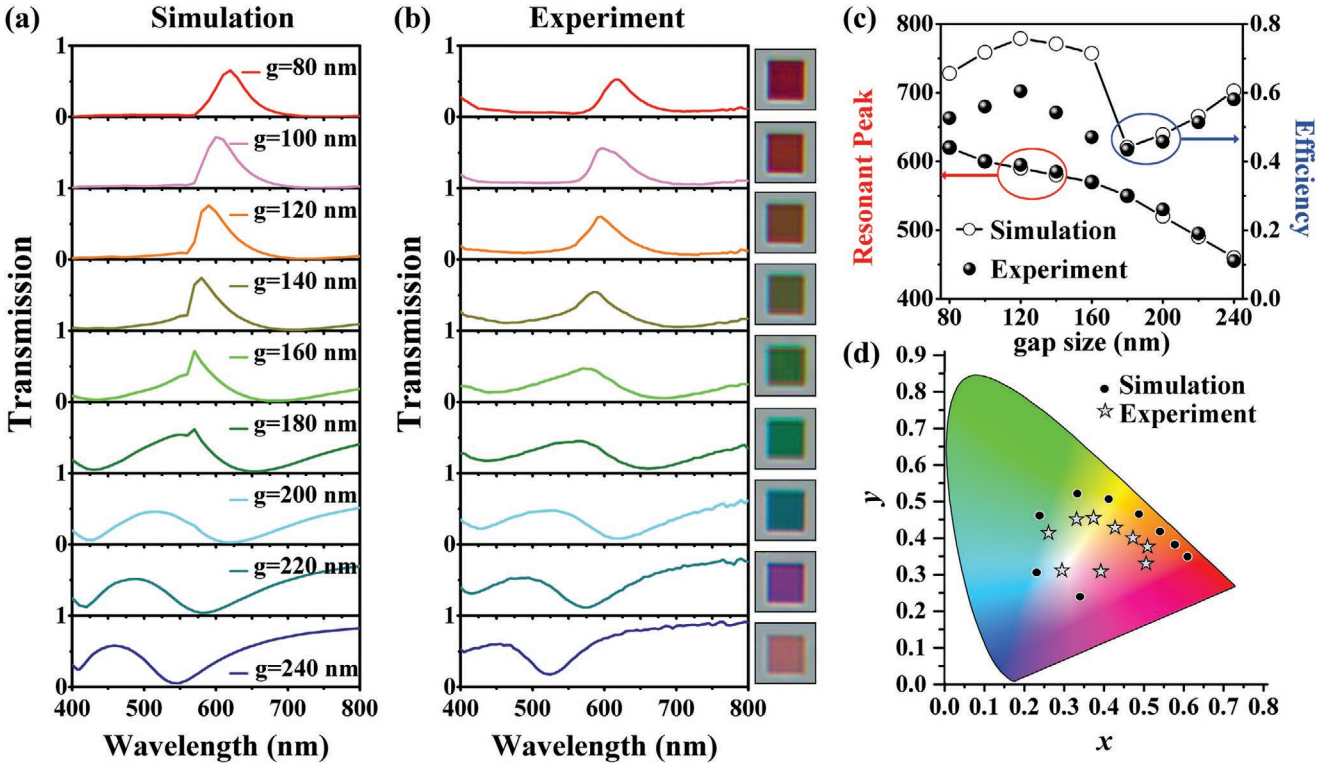

Figure 5. Structural colors with full hue when the period is fixed at 380 nm for Al-Si_3N_4 metasurfaces. a) Simulated and b) measured transmission spectra when the gap size increases ranging from 80 to 240 nm with 20 nm increment. The insets show the measured color patterns, which changes from purple to red. c) The comparison between simulated and measured results in the aspects of locations (red arrow) and efficiency (blue arrow) of resonant peak. d) 1931 CIE diagram for corresponding simulated (black dots) and measured (grey stars) spectra in (a) and (b), implying that hybrid Al-Si_3N_4 metasurface can cover full hue with constant resolutions.

difference and make the resonant peak move to the longer wavelength.[34] On the other hand, with the increasing of gap size, the coupling between neighboring hybrid nanoblocks is progressively reduced, resulting in gradually widening FWHM of spectra and decreasing transmission efficiency. The diminished coupling between Mie lattice resonances and Wood's anomaly can also lead to relieving suppression for transmission efficiency at nonresonant wavelengths. That means the monochromaticity of transmission spectra will gradually decrease with the blue shift of resonant peak when gap size increases from 80 to 240 nm. Even so, a wide gamut consisting of three primary colors in RGB model can be successfully realized at a constant period. Figure 5b exhibits the color patterns as the gap size increases every 20 nm. The vivid and wide-hue colors including pink, purple, blue, green, and red can be successively realized. We quantitatively compared the simulated and measured resonant peaks and their efficiencies in Figure 5c, which are consistent with each other. The 1931 CIE diagram in Figure 5d intuitively presents the simulated and measured color gamut at a constant period. Although the saturation for the blue-green range is relatively lower compared with red color, which is in accordance with predication, full-hue colors can be obtained both in simulation and experiment. In a word, the proposed hybrid Al-Si_3N_4 nanostructures can realize the full-hue colors with constant resolutions in transmission mode, which is crucial for practical applications.

2.3. The Property of Incident Angle Dependence

The excited light is not always normally incident to the sample in many cases, which are important in practical display applications. We therefore studied the effects of the incident angles on the performances of the structural colors realized by proposed hybrid Al-Si_3N_4 nanostructures. The definitions of the tilted incidence under *s* and *p*-polarization states are shown in **Figures 6**a and 6b, respectively. We plotted the simulated transmission spectra as a function of incident angle for both *s* and *p*-polarization states in Figures 6c and 6d, where the period and gap size are fixed at 330 and 80 nm, respectively. For the case of *s*-polarization state, the uniform transmission peak is limited within wavelength of 515–535 nm when the incident angle spans from 0° to 30°, indicating high insensitivity for incident angle. In contrast, the transmission peak experiences a dramatic redshift from 535 to 800 nm under *p*-polarization state along with the tilted incident angle, which can be attributed to decreasing electric component parallel to the top surface resulting from the increasing of incident angle. Overall, the incident-angle tolerance of the designed

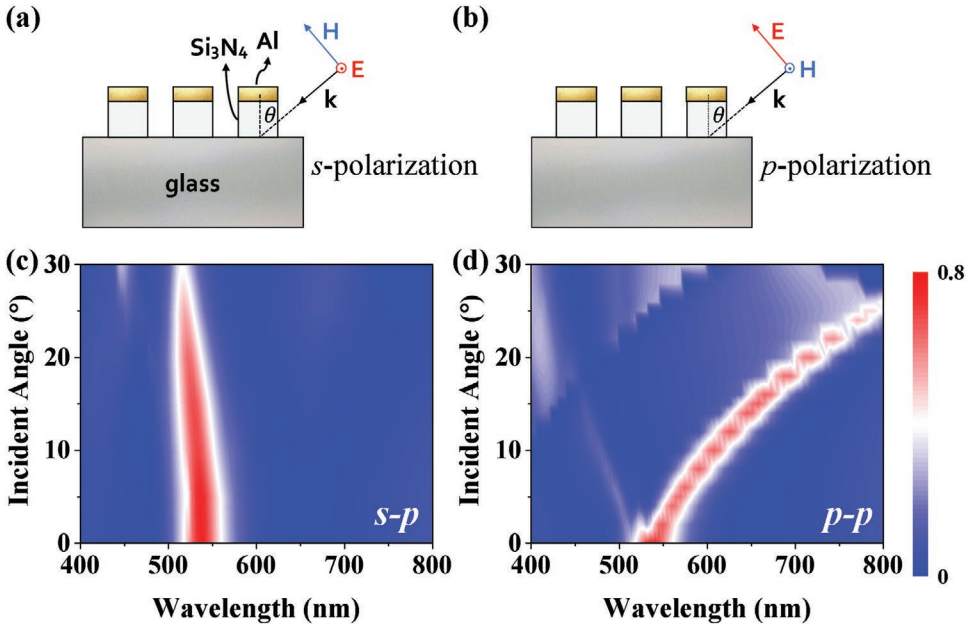

Figure 6. The angle-dependence of Al-Si_3N_4 metasurfaces. a,b) Schematic of tilted incidence under a) *s*-polarization and b) *p*-polarization states. c,d) Contour map of simulated transmission spectra as a function of incident angle and wavelength under c) *s*-polarization and d) *p*-polarization states, respectively.

hybrid Al-Si_3N_4 nanostructures can reach 30° under *s*-polarization state.

3. Conclusion

In conclusion, we have proposed and demonstrated the high-performance transmission structural colors in RGB model with high saturation, full hue, high efficiency, easy manufacturability, and polarization independence by using unique hybrid Al-Si_3N_4 nanostructures. The strategy of adding Si_3N_4 layer beneath Al nanoblocks can introduce magnetic-dipole and electric-quadrupole resonances given by the coupling between Wood's anomaly and Mie lattice resonance, leading to enhanced efficiency and monochromaticity of transmission spectra. High-saturation and full-hue colors are realized both in simulation and experiment resulting from high-monochromaticity spectra with efficiency of 70% and FWHM of 50 nm. By tuning the geometrical parameters, wide gamut taking up 150% sRGB space can be obtained in simulation, which is superior to previous studies on transmission colors. Besides, we have proved full-hue colors within constant resolutions, indicating the hybrid metal-dielectric nanostructures have potential for displaying and imaging applications.

Acknowledgements

This work was supported by the National Key Research and Development Program of China (2016YFA0301102 and 2017YFA0303800), the National Natural Science Fund for Distinguished Young Scholars (11925403), the National Natural Science Foundation of China (11974193, 11904181, 11904183, 91856101, and 11774186), and the Natural Science Foundation of Tianjin for Distinguished Young Scientists (18JCJQJC45700).

Conflict of Interest

The authors declare no conflict of interest.

Data Availability Statement

The data that support the findings of this study are available from the corresponding author upon reasonable request.

Keywords

high saturation, metal-dielectric metasurfaces, Mie lattice resonances, transmission colors, Wood's anomaly

Received: May 5, 2021
Revised: July 11, 2021
Published online:

[1] M. K. Hedayati, M. Elbahri, *Plasmonics* **2017**, *12*, 1463.
[2] A. Kristensen, J. K. W. Yang, S. I. Bozhevolnyi, S. Link, P. Nordlander, N. J. Hales, N. A. Mortensen, *Nat. Rev. Mater.* **2017**, *2*, 16088.
[3] Y. Gu, L. Zhang, J. K. Yang, S. P. Yeo, C. W. Qiu, *Nanoscale* **2015**, *7*, 6409.
[4] S. Daqiqeh Rezaei, Z. Dong, J. You En Chan, J. Trisno, R. J. H. Ng, Q. Ruan, C.-W. Qiu, N. A. Mortensen, J. K. W. Yang, *ACS Photonics* **2021**, *8*, 18.
[5] K. Baek, Y. Kim, S. Mohd-Noor, J. K. Hyun, *ACS Appl. Mater. Interfaces* **2020**, *12*, 5300.
[6] B. Yang, H. Cheng, S. Chen, J. Tian, *Mater. Chem. Front.* **2019**, *3*, 750.
[7] X. M. Goh, Y. Zheng, S. J. Tan, L. Zhang, K. Kumar, C. W. Qiu, J. K. W. Yang, *Nat. Commun.* **2014**, *5*, 5361.

[8] J. Olson, A. Manjavacas, L. Liu, W. S. Chang, B. Foerster, N. S. King, M. W. Knight, P. Nordlander, N. J. Halas, S. Link, *Proc. Natl. Acad. Sci. U. S. A.* **2014**, *111*, 14348.
[9] M. Miyata, H. Hatada, J. Takahara, *Nano Lett.* **2016**, *16*, 3166.
[10] H. Wang, X. Wang, C. Yan, H. Zhao, J. Zhang, C. Santschi, O. J. Martin, *ACS Nano* **2017**, *11*, 4419.
[11] X. M. Goh, R. J. H. Ng, S. Wang, S. J. Tan, J. K. W. Yang, *ACS Photonics* **2016**, *3*, 1000.
[12] X. Zhu, C. Vannahme, E. Højlund-Nielsen, N. A. Mortensen, A. Kristensen, *Nat. Nanotechnol.* **2016**, *11*, 325.
[13] C. U. Hail, G. Schnoering, M. Damak, D. Poulikakos, H. Eghlidi, *ACS Nano* **2020**, *14*, 1783.
[14] B. Gholipour, G. Adamo, D. Cortecchia, H. N. Krishnamoorthy, M. D. Birowosuto, N. I. Zheludev, C. Soci, *Adv. Mater.* **2017**, *29*, 1604268.
[15] Y. Nagasaki, M. Suzuki, J. Takahara, *Nano Lett.* **2017**, *17*, 7500.
[16] Z. Dong, J. Ho, Y. F. Yu, Y. H. Fu, R. Paniagua-Dominguez, S. Wang, A. I. Kuznetsov, J. K. W. Yang, *Nano Lett.* **2017**, *17*, 7620.
[17] S. Sun, Z. Zhou, C. Zhang, Y. Gao, Z. Duan, S. Xiao, Q. Song, *ACS Nano* **2017**, *11*, 4445.
[18] B. Yang, W. Liu, Z. Li, H. Cheng, S. Chen, J. Tian, *Adv. Opt. Mater.* **2018**, *6*, 1701009.
[19] B. Yang, W. Liu, Z. Li, H. Cheng, D. Y. Choi, S. Chen, J. Tian, *Nano Lett.* **2019**, *19*, 4221.
[20] J. H. Yang, V. E. Babicheva, M. W. Yu, T. C. Lu, T. R. Lin, K. P. Chen, *ACS Nano* **2020**, *14*, 5678.
[21] W. Yang, S. Xiao, Q. Song, Y. Liu, Y. Wu, S. Wang, J. Yu, J. Han, D. P. Tsai, *Nat. Commun.* **2020**, *11*, 1864.
[22] P. Hosseini, C. D. Wright, H. Bhaskaran, *Nature* **2014**, *511*, 206.
[23] S. G.-C. Carrillo, L. Trimby, Y.-Y. Au, V. K. Nagareddy, G. Rodriguez-Hernandez, P. Hosseini, C. Ríos, H. Bhaskaran, C. D. Wright, *Adv. Opt. Mater.* **2019**, *7*, 1801782.
[24] O. Hemmatyar, S. Abdollahramezani, S. Lepeshov, A. Krasnok, T. Brown, A. Alu, A. Adibi, arXiv: 2105.01313.
[25] V. R. Shrestha, S. S. Lee, E. S. Kim, D. Y. Choi, *Nano Lett.* **2014**, *14*, 6672.
[26] M. Ye, L. Sun, X. Hu, B. Shi, B. Zeng, L. Wang, J. Zhao, S. Yang, R. Tai, H. J. Fecht, J. Z. iang, D. X. Zhang, *Opt. Lett.* **2015**, *40*, 4979.
[27] L. Duempelmann, A. Luu-Dinh, B. Gallinet, L. Novotny, *ACS Photonics* **2016**, *3*, 190.
[28] R. Yu, P. Mazumder, N. F. Borrelli, A. Carrilero, D. S. Ghosh, R. A. Maniyara, D. Baker, F. J. G. De Abajo, V. Pruneri, *ACS Photonics* **2016**, *3*, 1194.
[29] V. Flauraud, M. Reyes, R. Paniagua-Dominguez, A. I. Kuznetsov, J. Brugger, *ACS Photonics* **2017**, *4*, 1913.
[30] D. Inoue, A. Miura, T. Nomura, H. Fujikawa, K. Sato, N. Ikeda, D. Tsuya, Y. Sugimoto, Y. Koide, *Appl. Phys. Lett.* **2011**, *98*, 093113.
[31] Z. Li, A. W. Clark, J. M. Cooper, *ACS Nano* **2016**, *10*, 492.
[32] Y. Lee, M. K. Park, S. Kim, J. H. Shin, C. Moon, J. Y. Hwang, J. C. Choi, H. Park, H. R. Kim, J. E. Jang, *ACS Photonics* **2017**, *4*, 1954.
[33] A. M. Shaltout, J. Kim, A. Boltasseva, V. M. Shalaev, A. V. Kildishev, *Nat. Commun.* **2018**, *9*, 2673.
[34] Y. Wang, M. Zheng, Q. Ruan, Y. Zhou, Y. Chen, P. Dai, Z. Yang, Z. Lin, Y. Long, Y. Li, N. Liu, C. W. Qiu, J. K. W. Yang, H. Duan, *Research* **2018**, *2018*, 8109054.
[35] J. G. Yun, J. Sung, S. J. Kim, H. Yun, C. Choi, B. Lee, *Sci. Rep.* **2019**, *9*, 15381.
[36] J. S. Lee, J. Y. Park, Y. H. Kim, S. Jeon, O. Ouellette, E. H. Sargent, D. H. Kim, J. K. Hyun, *Nat. Commun.* **2019**, *10*, 4782.
[37] C. H. Park, Y. T. Yoon, V. R. Shrestha, C. S. Park, S. S. Lee, E. S. Kim, *Opt. Express* **2013**, *21*, 28783.
[38] H. Kim, M. Kim, T. Chang, A. Baucour, S. Jeon, N. Kim, H. J. Choi, H. Lee, J. Shin, *Opt. Express* **2018**, *26*, 27403.
[39] M. Sarrazin, J.-P. Vigneron, J.-M. Vigoureux, *Phys. Rev. B* **2003**, *67*, 085415.
[40] D. De Ceglia, M. A. Vincenti, M. Scalora, N. Akozbek, M. J. Bloemer, *AIP Adv.* **2011**, *1*, 032151.
[41] X. Jia, P. Bowen, Z. Huang, X. Liu, C. Bingham, D. R. Smith, *Opt. Express* **2018**, *26*, 3004.
[42] T. Kaelberer, V. A. Fedotov, N. Papasimakis, D. P. Tsai, N. I. Zheludev, *Science* **2010**, *330*, 1510.
[43] A. Arbabi, A. Faraon, *Sci. Rep.* **2017**, *7*, 43722.
[44] Y. Zhang, H. Liu, H. Cheng, J. Tian, S. Chen, *Opto-Electron. Adv.* **2020**, *3*, 200002.